

Article

# Terahertz Metamaterial Waveguide with I-Shaped Resonators for Phase and Absorption Modulation

Bo Yu <sup>1</sup> , Jie Yang <sup>2</sup>, Yexi Song <sup>2</sup>, Zhigang Wang <sup>1,\*</sup>, Tiedi Zhang <sup>1</sup>, Bo Yan <sup>1,\*</sup> and Ruimin Xu <sup>1</sup>

<sup>1</sup> School of Electronic Science and Engineering, University of Electronic Science and Technology of China, Chengdu 611731, China; yubo21@std.uestc.edu.cn (B.Y.)

<sup>2</sup> Sichuan Jiuzhou Electric Group Co., Ltd., Mianyang 621000, China; yangjie@jezetek.cc (J.Y.)

\* Correspondence: zhigangwang@uestc.edu.cn (Z.W.); yanbo@uestc.edu.cn (B.Y.)

**Abstract:** In terahertz communication systems, amplifiers and other components can induce non-linear distortion in terms of amplitude and phase, resulting in system performance degradation. This paper presents a terahertz metamaterial waveguide to mitigate amplitude and phase distortions in some terahertz systems. A simple method based on free-space analysis is proposed for designing metamaterial waveguides in an enclosed space. The quasi-periodic metamaterial structures, which feature I-shaped resonant patterns, are integrated onto the inner walls of rectangular waveguides. The phase and amplitude of electromagnetic waves within the waveguide can be modulated by varying the dimensions and number of these resonators. Utilizing the effective medium theory and the equivalent circuits, the metamaterial waveguide's phase and absorption modulation mechanisms are analyzed. Based on the proposed structure, a metamaterial waveguide with I-shaped resonators is designed and fabricated, and its abilities to modulate the phase and absorption of terahertz waves around 0.2 THz are demonstrated.

**Keywords:** metamaterials; waveguides; I-shaped resonators; absorption; phase



**Citation:** Yu, B.; Yang, J.; Song, Y.; Wang, Z.; Zhang, T.; Yan, B.; Xu, R. Terahertz Metamaterial Waveguide with I-Shaped Resonators for Phase and Absorption Modulation.

*Photonics* **2023**, *10*, 816. <https://doi.org/10.3390/photonics10070816>

Received: 20 June 2023

Revised: 7 July 2023

Accepted: 11 July 2023

Published: 13 July 2023



**Copyright:** © 2023 by the authors. Licensee MDPI, Basel, Switzerland. This article is an open access article distributed under the terms and conditions of the Creative Commons Attribution (CC BY) license (<https://creativecommons.org/licenses/by/4.0/>).

## 1. Introduction

Terahertz technology has exhibited significant potential in high-speed wireless communication [1,2], high-precision imaging [3,4], and astronomical detection [5]. Various terahertz devices have been developed, including filters [6], mixers [7], absorbers [8], and polarizers [9]. However, in the terahertz communication system, distortion in both amplitude and phase can be caused by large gain fluctuations and nonlinear phase variations in some components like power amplifiers [10,11], thereby decreasing communication performance. Therefore, it is necessary to design a terahertz modulator that can regulate and compensate for both the amplitude and phase.

Electromagnetic metamaterials, consisting of periodically arranged artificial microstructure arrays, can enable unique electromagnetic properties and manipulate electromagnetic waves [12]. Many investigations on the properties and applications of metamaterials have been reported, including terahertz magnetic response [13], negative refraction [14], microwave electromagnetic cloak [15], super-lenses [16], and perfect absorbers [8,17,18]. Additionally, broadband metamaterial absorbers with fractal geometric structures have been proposed, such as a hexagonal nano-ring fractal configuration [19], a Pythagorean-tree fractal geometry [20], and an elliptical arrangement of metallic rings in a fractal structure [21]. Furthermore, some terahertz phase modulators [22–24] based on metamaterials have been developed for manipulating radiation. However, most reported metamaterial devices are simulated, designed, and operated in free space. It is difficult to eliminate the scattering effects in free space, which can introduce measurement errors and increase the losses of metamaterial devices. Furthermore, integrating the metamaterial devices operating in free space with terahertz systems is also challenging.

In terahertz systems, rectangular waveguides are important transmission lines for designing passive devices such as filters, power splitters, and couplers. They can confine electromagnetic waves entirely within an enclosed space [25]. Rectangular waveguides are also considered as the most suitable interface for terahertz packages due to their low loss, wide bandwidth, and durability. Therefore, integrating metamaterials with rectangular waveguides to form an enclosed metamaterial waveguide can avoid free-space scattering and facilitate the integration and interconnection with terahertz systems. Despite the reports of incorporating metasurfaces in photonic integrated circuits to control guided waves [26,27], integrating metamaterials into metallic waveguides differs significantly from photonic integrated devices regarding the circuit structure, characteristics, operating frequency bands, and application domains.

In recent years, a variety of metamaterial waveguides have been proposed to achieve different functionalities and applications, including waveguide filters [28], a customizable equalizer [29], terahertz waveguide modulators [30], a susceptible permittivity sensor [31], and light storage [32]. These studies have brought promising prospects to the field of metamaterial waveguides. However, research on metamaterial waveguides operating in the 0.2 THz band remains relatively limited. This particular frequency band is located in the so-called atmospheric window, where the propagation attenuation is minimized, allowing superior wireless transmission [33]. High-speed wireless communication systems operating in the 0.2 THz frequency band have been developed [34,35]. However, there remains a lack of corresponding metamaterial waveguides that can achieve simultaneous phase and absorption modulation. As illustrated in Figure 1, this type of metamaterial waveguide can be utilized in 0.2 THz satellite communication systems to regulate both amplitude and phase, thereby enhancing system performance. As depicted in Figure 2, the nonlinear transmission characteristics exhibited by the metamaterial waveguide can be regarded as an inversion of the system's transmission response in both amplitude and phase, thereby allowing the system to maintain a linear phase and a flat amplitude response.

In this study, a metamaterial waveguide capable of achieving phase and absorption modulation has been proposed to address amplitude and phase distortions in terahertz systems. The metamaterial waveguide is constructed by placing a quartz substrate with quasi-periodic structures on the inner wall of the rectangular waveguide. Simple I-shaped resonators are utilized as the fundamental resonant structures in the metamaterial waveguide. By altering the number and dimension of the I-shaped resonators, control over the phase and absorption of electromagnetic waves within the waveguide can be achieved. Consequently, a corresponding metamaterial waveguide can be designed to improve the amplitude and phase distortions based on the characteristics of the terahertz communication system. In addition, an equivalent media model and an equivalent circuit model of the metamaterial waveguide are established in the second section to analyze the modulation mechanisms of the waveguide's phase and absorption. The metamaterial waveguide is also explored through full-wave electromagnetic simulation in the third section. Finally, the phase and amplitude modulation of the metamaterial waveguide around 0.2 THz is demonstrated through fabrication and measurement.

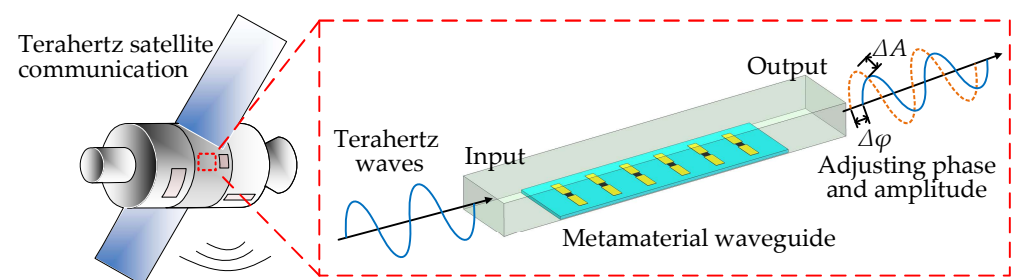


**Figure 1.** Applications of metamaterial waveguides in satellite communication systems to mitigate amplitude and phase distortions.

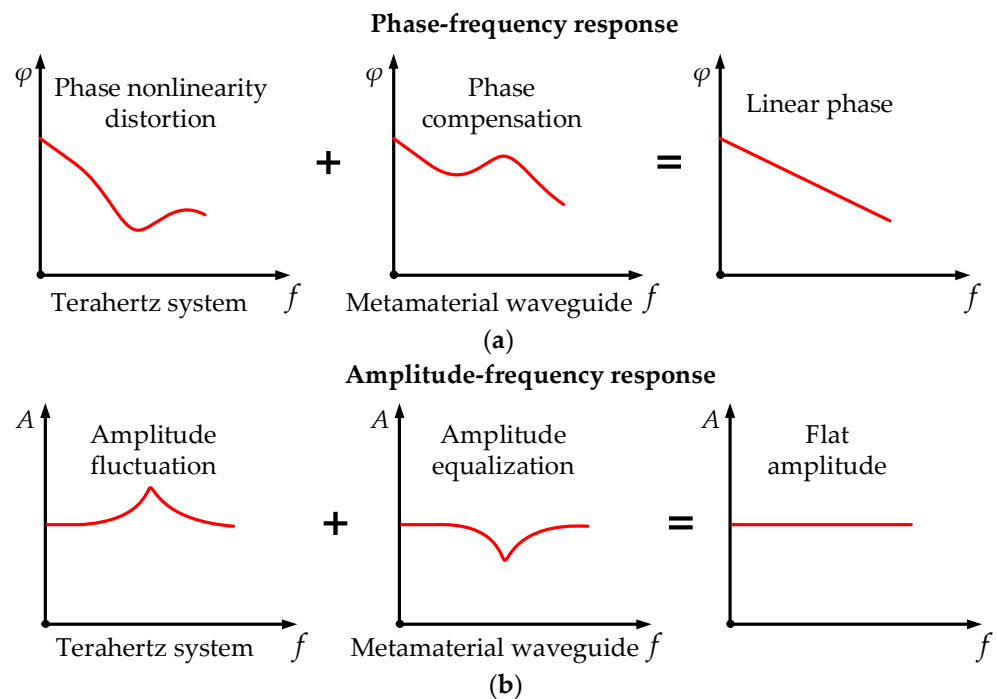


**Figure 2.** The metamaterial waveguide’s response is the opposite of the system’s response in both magnitude and phase. (a) Phase compensation. (b) Amplitude equalization.

**2. Principle and Design**

In free space, it has been demonstrated that metamaterials based on artificial periodic structures can manipulate electromagnetic waves in the terahertz bands [12]. A metal–dielectric–metal laminated structure [36] is one of the most commonly used structures in metamaterial design. The top layer consists of sub-wavelength resonant patterns arranged periodically, the middle layer is a dielectric layer, and the bottom layer is a metal plane. Based on the metal–dielectric–metal laminated structure, a simple method is proposed to design the metamaterial from infinite free space transformation to an enclosed space. Additionally, metamaterials often employ symmetric resonant structures in free space to ensure their consistent response to electromagnetic waves incident from any direction [19]. However, in the rectangular waveguide, the propagation direction and polarization state of electromagnetic waves are constrained by the geometric structure and remain fixed [37]. Therefore, there is no necessity to use symmetric resonators in the metamaterial waveguide design.

Figure 3 illustrates the proposed terahertz metamaterial waveguide’s design and evolution process diagram. A two-dimensional (2D) metamaterial is first designed and simulated in free space and subsequently degraded into a one-dimensional linear array and integrated into a rectangular waveguide. As shown in Figure 3a, a quartz substrate is selected as the dielectric layer, and a simple I-shaped metallic line is initially chosen as the top resonant pattern. Then, a gap is introduced in the I-shaped line to facilitate resonance excitation, splitting it into two symmetric halves. The metallic gap of the I-shaped resonator forms an equivalent gap capacitor, enhancing the resonance effect. To improve the I-shaped resonator’s performance in absorbing and manipulating electromagnetic waves, a resistive loss material is added to the metallic gap [29]. The added loss material is a TaN thin-film resistor with a resistance  $R_0$  of 50 or 100 ohms in a square shape of any size. The resistance value of the thin-film resistor is determined by its width and length and can be calculated with the formula  $R = R_0 \times (g/w_R)$ . The geometrically simple structure of the I-shaped resonator can also simplify the design and manufacturing.

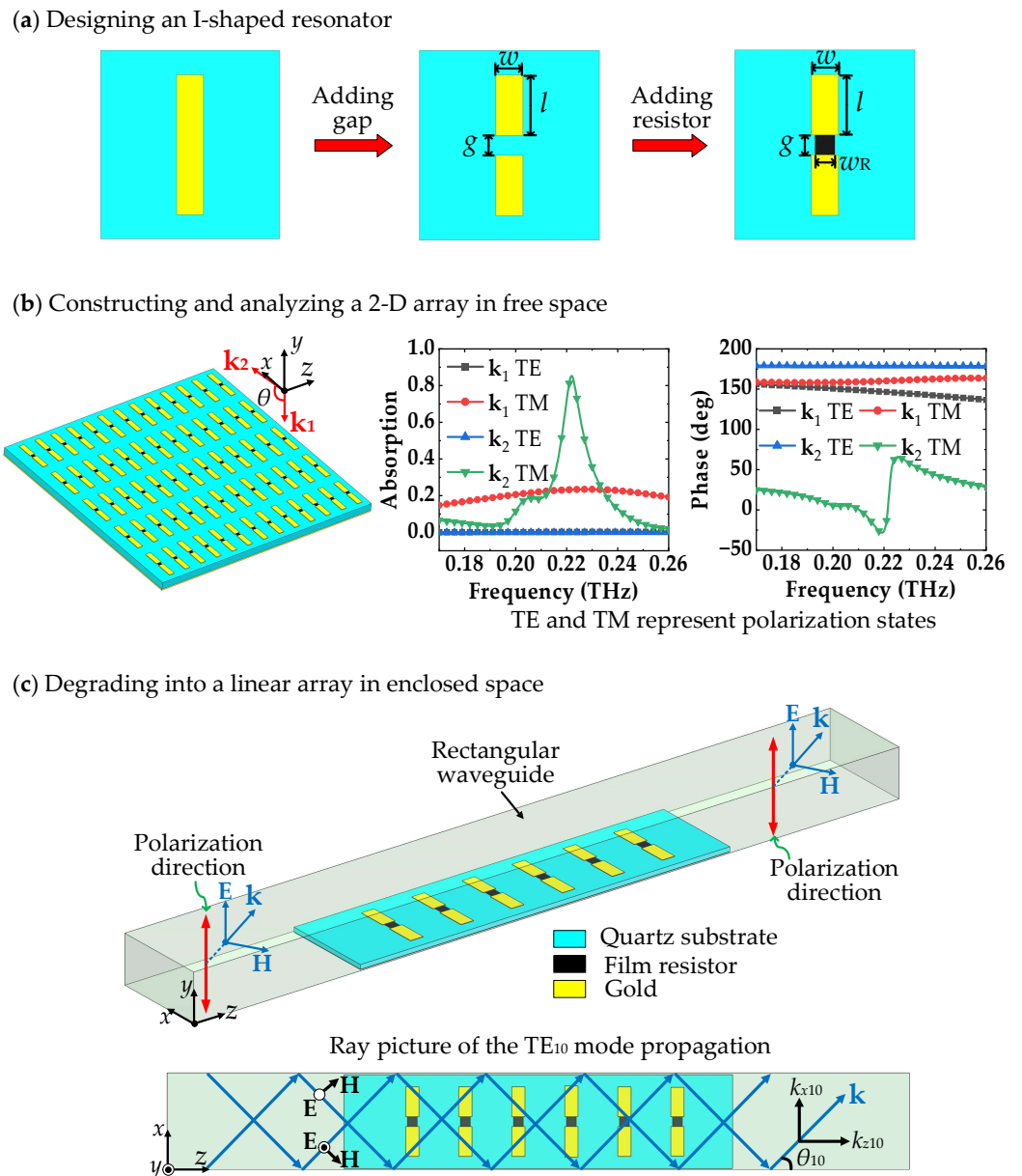


**Figure 3.** Design and evolution process diagram of the proposed metamaterial waveguide.

Next, as depicted in Figure 3b, arranging the I-shaped resonators periodically in a 2D plane creates a metamaterial operating in free space. Simulations are performed by directing the incident wave perpendicular or nearly parallel ( $\theta = 88^\circ$ ) to the plane to obtain the metamaterial’s absorption and phase modulation characteristics under the TE and TM polarization states. Maintaining a small elevation angle during parallel incidence ensures that the electromagnetic waves can act on the metamaterial during simulation. The simulation results in Figure 3b demonstrate that, in free space, this 2D metamaterial can modulate the phase and amplitude of TM-polarized electromagnetic waves that are nearly parallel to the plane.

Finally, an enclosed-space metamaterial structure is established by degrading the 2D metamaterial structure into a quasi-periodic linear array and integrating it into a metal waveguide. Figure 3c shows that the quartz substrate is placed on the broad bottom face of the rectangular waveguide, and the propagation direction of the electromagnetic waves within the waveguide is parallel to the substrate. This configuration can ensure that the proposed metamaterial waveguide has similar absorption and phase characteristics to the 2D metamaterial. Moreover, the fundamental transmission mode of the rectangular

waveguide is the TE<sub>10</sub> mode, in which the electric field is always perpendicular to the *xz*-plane, with no electric field in the propagation direction [37,38]. Consequently, the polarization direction of the electromagnetic wave is always perpendicular to the *xz*-plane. The field of the TE<sub>10</sub> mode can be decomposed into two plane waves of equal amplitude propagating in two different directions in the *xz*-plane [37], as illustrated in Figure 3(c). The angle between the propagation direction and the *z*-axis is given by  $\theta_{10} = \tan^{-1}(k_{x10}/k_{z10})$ , where the  $k_{x10}$  and  $k_{z10}$ , respectively, denote the propagation constants of the TE<sub>10</sub> mode along the *x*-axis and the *z*-axis. Therefore, the propagation direction and polarization state of electromagnetic waves are fixed in the metamaterial waveguide.

Figure 4a displays the cross-sectional view of the terahertz metamaterial waveguide. The width and height of the WR-4.3 standard rectangular waveguide are, respectively, 1092 μm and 546 μm. The substrate comprises a 50 μm thick quartz layer, two 4 μm thick layers of gold, and approximately 40 nm thick TaN thin-film resistors. The dielectric constant of the quartz substrate is 3.82, and the refractive index is 1.95. The conductivity of the gold is  $4.1 \times 10^8 \text{ S m}^{-1}$ .

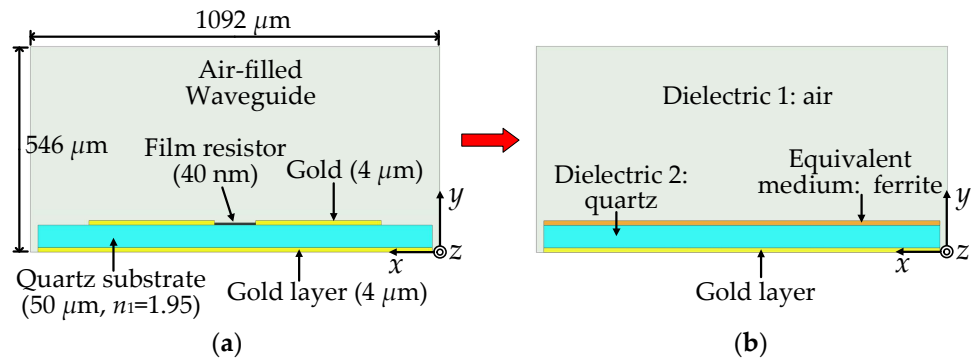


**Figure 4.** Cross-sectional view of (a) the terahertz metamaterial waveguide and (b) its equivalent medium model.

Based on the equivalent medium theory [39,40], periodically arranged I-shaped resonators can be regarded as an equivalent homogeneous ferrite layer, as illustrated in Figure 4b. According to Maxwell’s equations and previous research [37,38,41], transverse electromagnetic fields within the waveguide induce currents throughout the I-shaped resonators. These induced currents stimulate an induced magnetic field, and the magnetic field’s intensity  $|H_{ind}|$  is determined by the dimensions of the metallic and thin-film resistors. This physical process can be equivalently described as follows: when a magnetic field is applied to a ferrite material, the magnetic moments within the ferrite are rearranged to produce an induced magnetic field [37,38]. Therefore, the metamaterial structure can be equivalent to a ferrite–dielectric–gold laminated structure.

In our previous work [41], the authors demonstrated that the phase constant  $\beta$  of a metamaterial waveguide, based on the equivalent ferrite–dielectric–gold laminated structure, is correlated with the induced magnetic field intensity  $|H_{ind}|$ . Meanwhile, the intensity of the induced magnetic field is determined by the dimensions of the metallic and thin-film resistors within the I-shaped resonators. Therefore, the relationship between the phase constant and the dimensions of the I-shaped resonators can be expressed as follows:

$$\beta \sim |H_{ind}| \sim w, g, l, \tag{1}$$

which suggests that adjusting the dimensions of the I-shaped resonators makes it possible to modulate the phase of electromagnetic waves within the waveguide.

To analyze the physical mechanism of electromagnetic wave absorption, an equivalent circuit model of the I-shaped resonator is illustrated in Figure 5. For the I-shaped resonator, the equivalent circuit model includes two planar capacitance  $C_{mi}$ , two inductive inductance  $L_{mi}$ , two ohmic resistance of the gold wires  $R_{mi}$ , a thin-film resistor  $R_{ei}$ , and a gap capacitance

$C_{ei}$ . The expressions for the equivalent circuit parameters [25] of the I-shaped resonator are listed in Table 1. In this table,  $\mu_0$  is the permeability of air,  $\epsilon_r$  is the dielectric constant of the quartz substrate,  $\epsilon_0$  is the dielectric constant of the air,  $\rho$  represents the resistivity of the gold,  $t_s$  is the thickness of the quartz substrate, and  $t_m$  is the thickness of the gold wire.

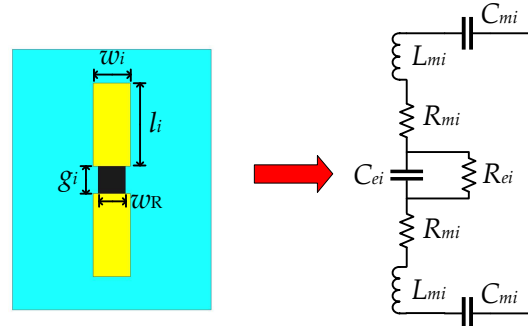


Figure 5. Equivalent circuit model of an I-shaped resonator.

Table 1. The expressions for the equivalent circuit parameters in Figure 5.

Parameters	$L_{mi}$	$C_{ei}$	$C_{mi}$	$R_{mi}$
Expression	$2 \frac{\mu_0 t_s}{w_i} l_i$	$\frac{\pi \epsilon_0 w_i}{2 \ln(g_i/t_m)}$	$\frac{\epsilon_0 \epsilon_r w_i}{t_s} l_i$	$\rho \frac{l_i}{w_i t_m}$

A 3D model and a cross-sectional view of a metamaterial waveguide with multiple I-shaped resonators are shown in Figure 6a. Its equivalent circuit model [42,43] is depicted in Figure 6b. The equivalent circuit of a single I-shaped resonator can be simplified as an RLC resonant circuit. Figure 7a depicts the opposing currents within the quartz substrate’s upper and lower metal layers. As illustrated in Figure 7b, the existence of the opposing currents is further validated by the electric field distribution in the  $xy$ -plane. Figure 7c shows the magnetic field distribution of the metamaterial waveguide in both the  $xy$ -plane and  $yz$ -plane. The reverse currents in the substrate’s upper and lower metal layers create magnetic dipoles and magnetic resonance. The quartz substrate absorbs energy under the effect of magnetic resonance, resulting in dielectric loss  $R_O$  [44,45]. Furthermore,  $R_i$  represents the total equivalent resistance of a resonator, including film resistors and the ohmic resistance of the gold wire.  $L_i$  is the total self-induced inductance and can be expressed as [25,46]:

$$L_i = 2L_{mi} = 2 \frac{\mu_0 t_s}{w_i} l_i, \quad i = 1, 2, 3, \dots, n. \tag{2}$$

Additionally, the total capacitance  $C_i$ , including two planar capacitance  $C_{mi}$  and a gap capacitance  $C_{ei}$ , can be expressed as [25,46]:

$$C_i = \frac{C_{ei} C_{mi}}{2C_{ei} + C_{mi}}, \quad i = 1, 2, 3, \dots, n. \tag{3}$$

Then, the resonant frequencies of the equivalent circuit model of the I-shaped metamaterial waveguide can be expressed as follows:

$$f_i = \frac{1}{2\pi \sqrt{L_i C_i}}, \quad i = 1, 2, 3, \dots, n. \tag{4}$$

The analysis of the equivalent circuit model and Equations (2)–(4) suggest that the absorption frequency and magnitude can be controlled by adjusting the dimensions of the I-shaped resonators. The power losses of the total equivalent resistance and dielectric loss determine the absorption magnitude.

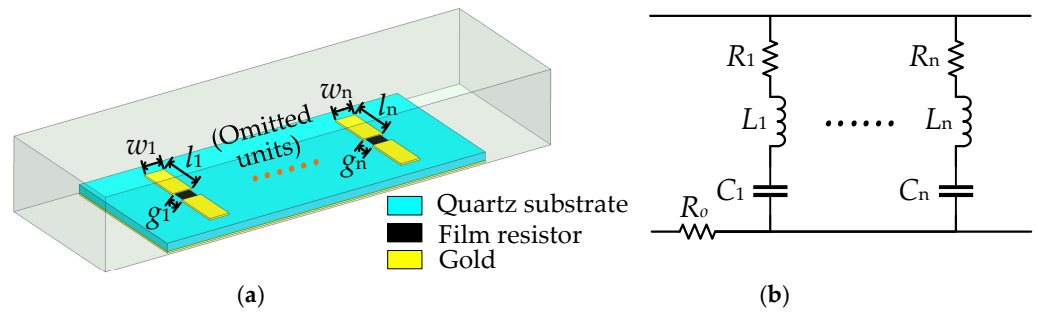


**Figure 6.** (a) A metamaterial waveguide with a finite number of quasi-periodic resonators (some of the resonators are omitted). (b) Equivalent circuit model of the metamaterial waveguide.

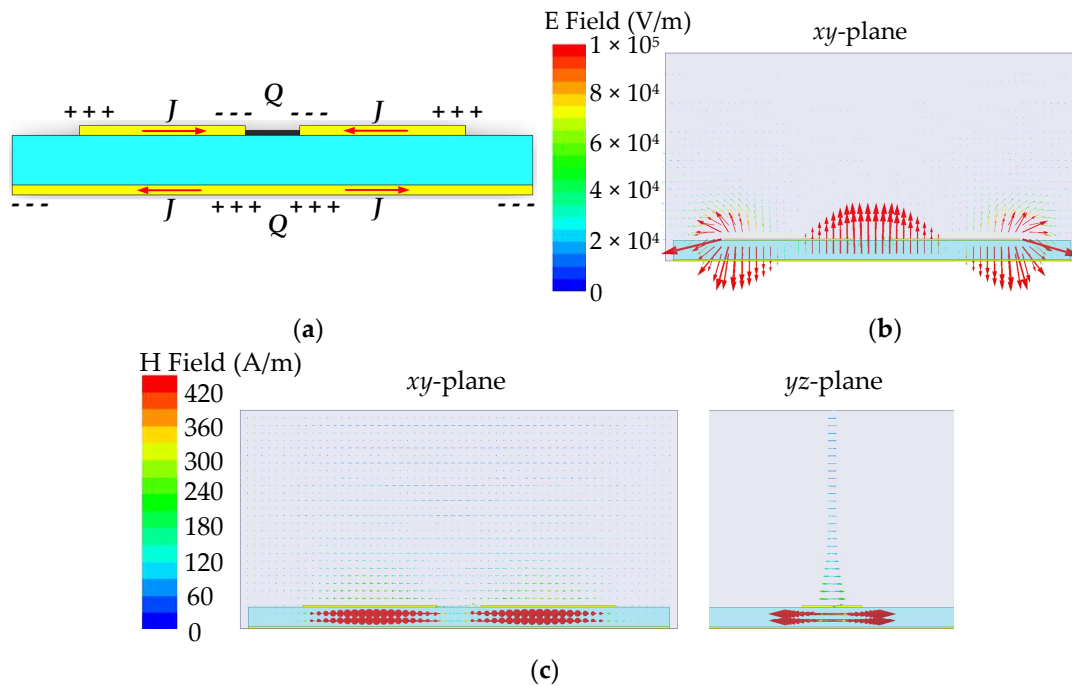


**Figure 7.** (a) The reverse currents within the upper and lower metal layers. (b) The electric field distribution in the  $xy$ -plane. (c) The magnetic field distribution in both the  $xy$ -plane and the  $yz$ -plane.

From the analysis in this section, by adjusting the dimensions of the gold wires and thin-film resistors within the I-shaped resonators, it is possible to manipulate the phase and amplitude of electromagnetic waves within the metamaterial waveguide. The following section will verify these findings through full-wave electromagnetic simulations.

### 3. Simulation and Analysis

A simulation model of the metamaterial waveguide with multiple I-shaped resonators is established in a high-frequency structure simulator (HFSS), as shown in Figure 8. A full-wave electromagnetic simulation was conducted on HFSS to validate the effectiveness of the proposed metamaterial waveguides. The dielectric constant of the 50  $\mu\text{m}$  thick quartz substrate is 3.82, and its dielectric loss tangent is 0.005. The conductivity of the 4  $\mu\text{m}$  thick layers of gold is  $4.1 \times 10^8 \text{ S m}^{-1}$ , and the resistivity of the thin-film resistance is  $100 \Omega \text{ sq}^{-1}$ . To simplify the simulation model, all the I-shaped resonators were set to the same size. The spacing between the units was set to  $s = 0.6 \text{ mm}$ . The initial dimensions of the metamaterial were as follows:  $w = 150 \mu\text{m}$ ,  $l = 335 \mu\text{m}$ ,  $g = 110 \mu\text{m}$ ,  $l_{\text{sub}} = 4400 \mu\text{m}$ , and  $w_{\text{sub}} = 1052 \mu\text{m}$ .

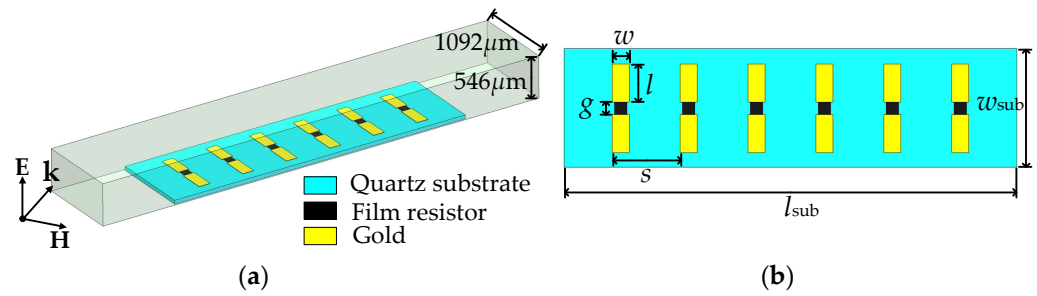


**Figure 8.** Simulation model on HFSS of the I-shaped metamaterial waveguide. (a) A 3D model. (b) The top view of the quartz substrate.

First, the phase and absorption of the metamaterial waveguide with different I-shaped resonator numbers are investigated in Figure 9a,b. As the number of resonators increases from 0 to 8, phase changes on both sides of 0.209 THz occur in opposite directions, while the amplitude of  $S_{21}$  gradually decreases. As a result, the phase and absorption of the metamaterial waveguide can be configured by controlling the number of resonators. The electric field distributions of the waveguide with  $N = 6$  at 0.2 THz and 0.209 THz are exhibited in Figure 9c,d. Compared to the result at 0.2 THz, the electric field intensity at the output port experiences a significant reduction at 0.209 THz, indicating a greater degree of absorption at this frequency.

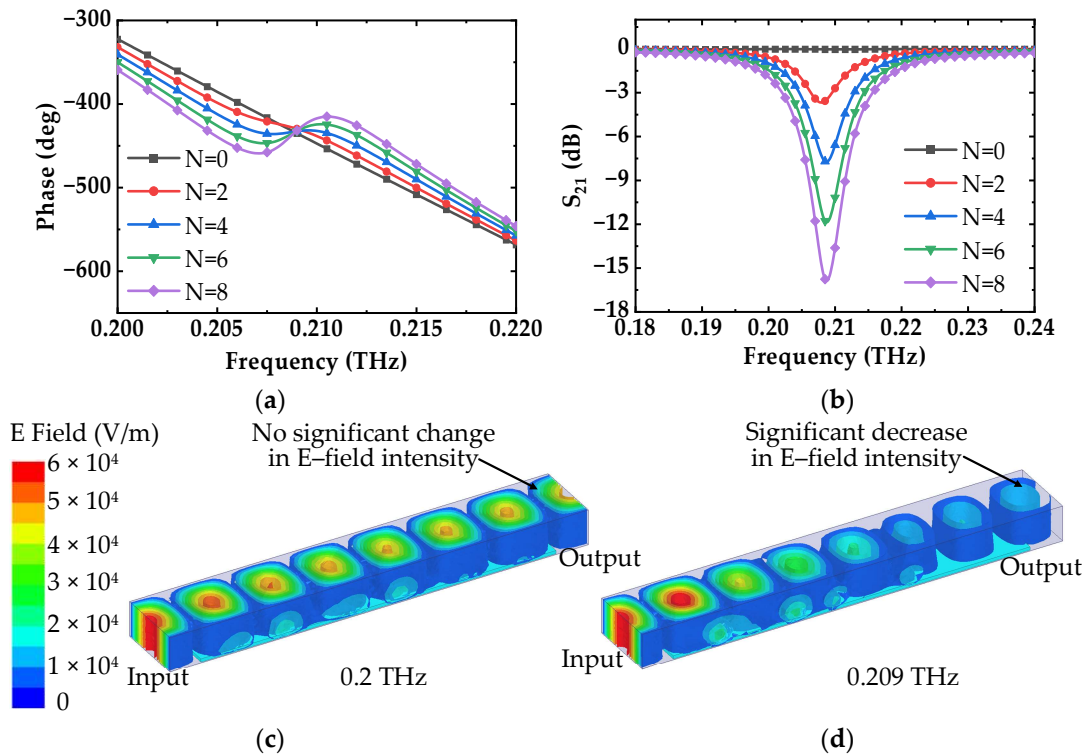


**Figure 9.** Simulated (a) phase and (b)  $S_{21}$  curves under different I-shaped unit numbers. (c) E-field distribution at 0.2 THz. (d) E-field distribution at 0.209 THz.

Second, with the number of resonators fixed at six, the effects of altering the dimensions of the gold wires and thin-film resistances on the phase and absorption are further investigated. As illustrated in Figure 10, by increasing the length of the gold wire from 305  $\mu\text{m}$  to 345  $\mu\text{m}$ , the absorption frequency significantly decreases, and the absorption amplitude gradually increases, with a maximum addition of 5.8 dB. Moreover, the phase change near each absorption frequency increases. According to Equations (2)–(4), it is evident that as the length of the gold wire increases, both the self-inductance and the planar capacitance increase, leading to a decrease in absorption frequency. Meanwhile, the

induced current and magnetic field intensity increase, resulting in an increase in both phase and absorption.

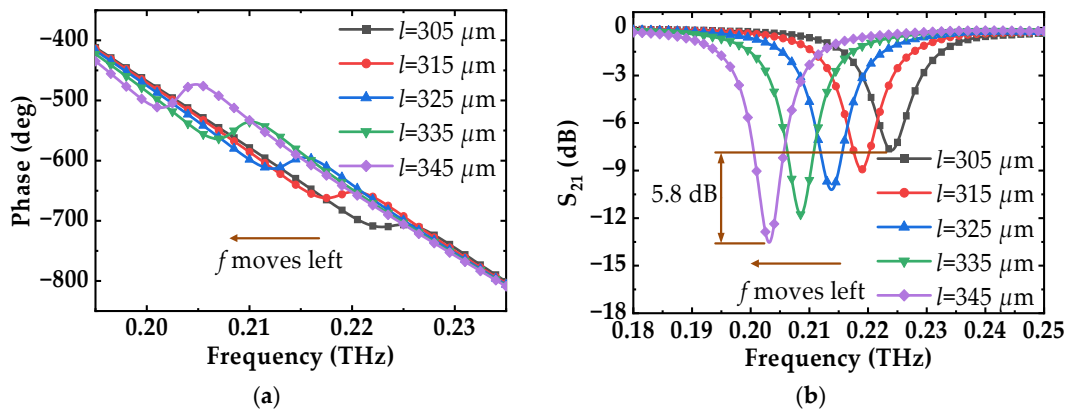


**Figure 10.** Simulated phase and absorption curves under different  $l$ . (a) Phase. (b)  $S_{21}$ . ( $f$  represents the absorption frequency).

Then, the effect of the gold wire width on phase and absorption is simulated in Figure 11. With an increase in the width of the gold wire from 120  $\mu\text{m}$  to 180  $\mu\text{m}$ , the phase gradually increases, reaching a maximum change of  $28^\circ$  at 209.6 GHz. Meanwhile, the absorption amplitude gradually increases, with a maximum increase of 5.8 dB at 208.7 GHz. The increase in the width of the gold wire leads to a corresponding increase in the induced current and magnetic field intensity, which in turn leads to greater coupling and interference of the electromagnetic waves within the metamaterial waveguide, resulting in a larger phase change. Furthermore, the increase in induced current elevates the losses of the thin-film resistance and dielectric, leading to increased absorption.

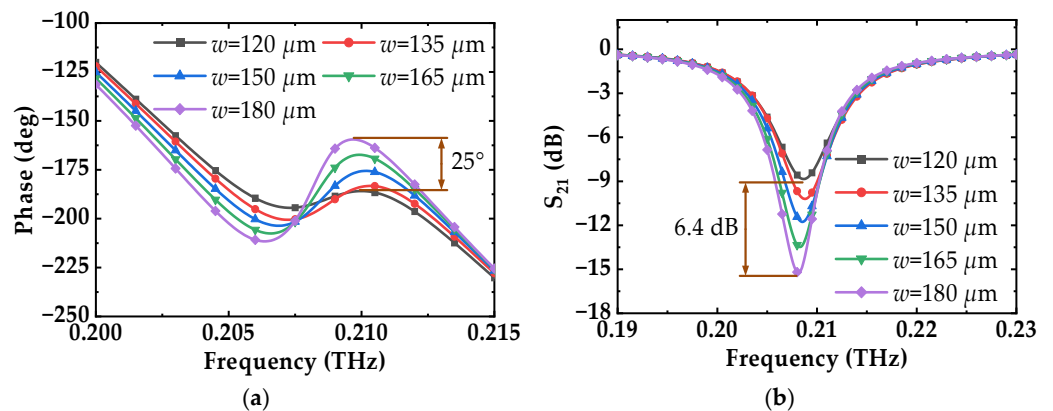


**Figure 11.** Simulated phase and absorption curves under different  $w$ . (a) Phase. (b)  $S_{21}$ .

Next, the influence of the length of thin-film resistance on phase and absorption is investigated in Figure 12. When the length of the thin-film resistor increases from 90  $\mu\text{m}$  to 130  $\mu\text{m}$  (the resistance value also increases gradually), the absorption frequency decreases, and the absorption amplitude gradually decreases, with a maximum reduction of 9.4 dB. Moreover, the phase change also gradually decreases. The reason is that when the thin-film resistance increases, the induced current reduces, and the loss of resistance and dielectric decreases, thus reducing absorption. At the same time, the induced magnetic field intensity also decreases, leading to a reduction in the phase change. Moreover, with an increase in the length of the thin-film resistance, the gap capacitance increases, as per Equations (2)–(4), which leads to a decrease in the absorption frequency.

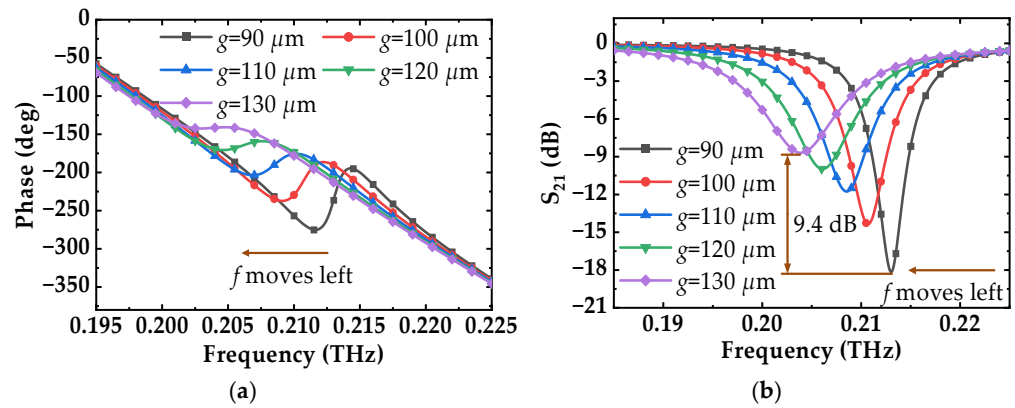


Figure 12. Simulated phase and absorption curves under different  $g$ . (a) Phase. (b)  $S_{21}$ .

In the above analysis, the I-shaped resonators are all set to the same size to simplify the HFSS model. However, a broadband response curve can be achieved when each I-shaped resonator has different dimensions and absorption frequencies. As depicted in Figure 13, the lengths of the six resonator unit cells increase sequentially from 275  $\mu\text{m}$  to 325  $\mu\text{m}$ , resulting in an accordingly leftward shift in their absorption frequencies. Figure 13b displays the simulated responses of the individual resonator units and the overall metamaterial waveguide. It can be observed that by strategically designing the absorption frequencies of each resonator unit cell, a broadband absorption curve is realized. In practical applications, adjusting each resonant unit’s length, width, and gap dimensions can achieve more complex phase and absorption curves to meet the system’s requirements.

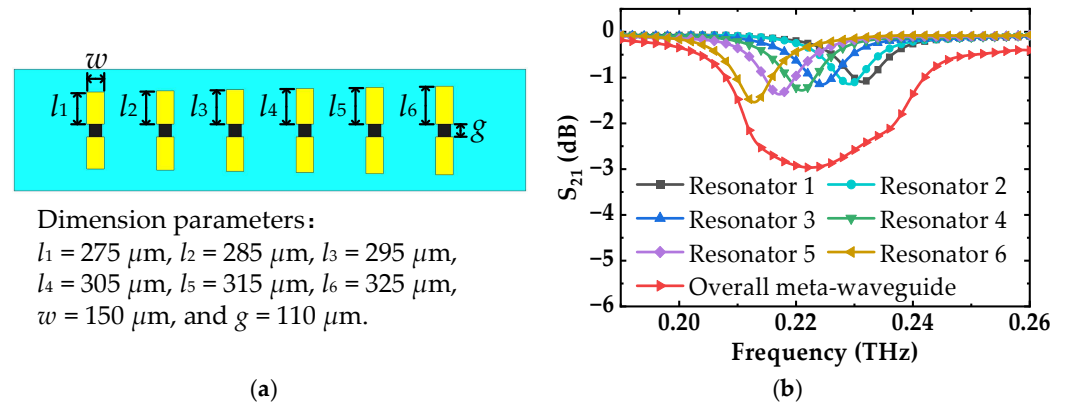


Figure 13. (a) The metamaterial consisting of I-shaped resonators with sequentially increasing lengths. (b) Simulated curves of each resonator and whole metamaterial waveguide.

To summarize, the lengths of the gold wire and thin-film resistance not only control the phase and absorption but can also change the absorption frequency. The width of the gold wire can adjust the phase and absorption but has little effect on the absorption frequency. Moreover, cascading multiple resonators with different dimensions makes it possible to achieve broadband phase and absorption characteristics. Based on these conclusions, the metamaterial waveguides can be designed according to the characteristics of the terahertz system, thereby achieving the desired phase and absorption. However, the proposed metamaterial waveguide has a limited phase shift range, and its phase is correlated with the absorption amplitude. Consequently, its applicability is also constrained and unable to meet the requirements of all terahertz systems. The presented metamaterial waveguide is primarily suitable for systems that require moderate phase correction while also necessitating energy absorption to improve amplitude flatness.

Additionally, further investigations have been carried out to explore the properties of metamaterial waveguides when replacing the I-shaped resonators with other shapes. As shown in Figure 14, the I-shaped resonators in the proposed metamaterial waveguide are

replaced with square-ring and cross-shaped resonators, respectively. The resistivities of the thin-film resistors in the resonators are  $100 \Omega \text{ sq}^{-1}$ . All the square-ring or cross-shaped resonators are set to the same size. The designed dimensions of these two metamaterial waveguides are as follows:  $w_r = 100 \mu\text{m}$ ,  $l_r = 335 \mu\text{m}$ ,  $g_r = 100 \mu\text{m}$ ,  $s_r = 1170 \mu\text{m}$ ,  $l_{\text{sub}1} = 7000 \mu\text{m}$ ,  $w_c = 100 \mu\text{m}$ ,  $l_c = 330 \mu\text{m}$ ,  $g_c = 130 \mu\text{m}$ ,  $s_c = 1100 \mu\text{m}$ ,  $l_{\text{sub}2} = 6500 \mu\text{m}$ , and  $w_{\text{sub}} = 1052 \mu\text{m}$ . The simulated results of these two metamaterial waveguides are depicted in Figure 15. Compared to the I-shaped resonators, the metamaterial waveguide with square-ring resonators exhibits dual absorption bands within the frequency range of 0.17 to 0.26 THz. Moreover, the metamaterial waveguide with cross-shaped resonators demonstrates higher absorption amplitude. Therefore, by introducing resonators of different shapes into the metamaterial waveguide, the characteristics can be altered, thereby expanding its range of applications.

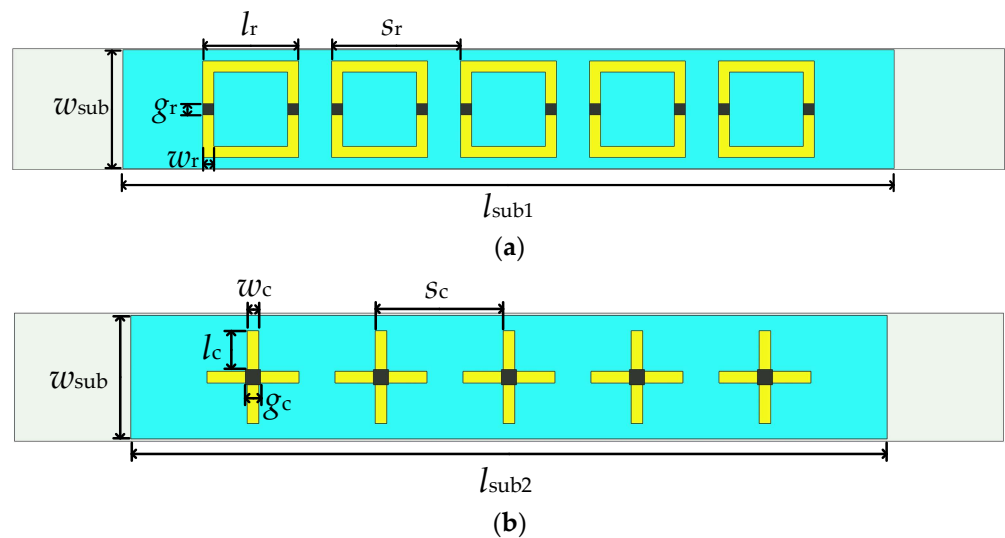


Figure 14. (a) The metamaterial waveguide with square-ring resonators. (b) The metamaterial waveguide with cross-shaped resonators.

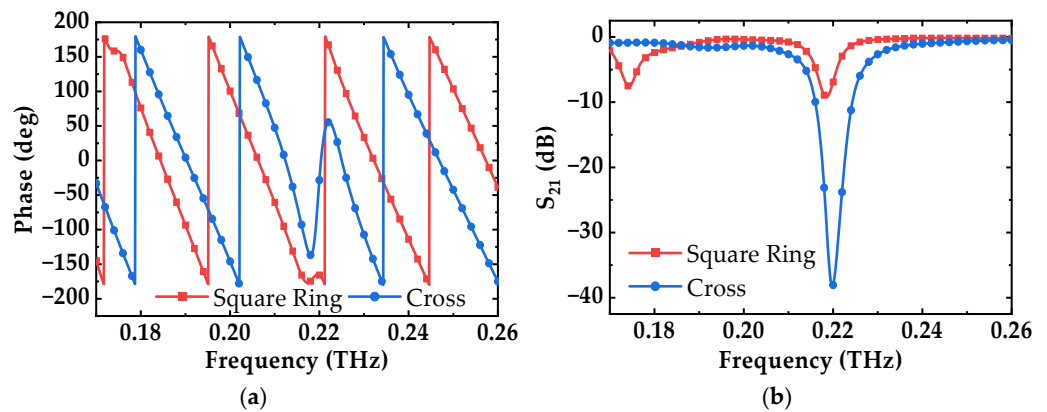
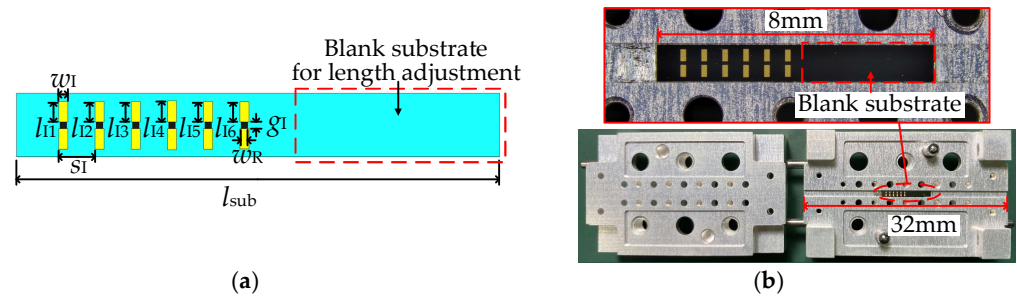


Figure 15. Simulated phase and absorption curves with square-ring and cross-shaped resonators. (a) Phase. (b)  $S_{21}$ .

#### 4. Experiments and Discussion

In terahertz communication systems, some devices, such as traveling-wave tube amplifiers, exhibit significant gain fluctuations and nonlinear phase variations, resulting in amplitude and phase distortion. Based on the previous analysis and simulation, the principle and characteristics of the proposed terahertz metamaterial waveguide have been obtained. In practical applications, corresponding metamaterial waveguides can be designed based on terahertz systems' characteristics to reduce amplitude and phase distortion.

An I-shaped metamaterial waveguide is designed and fabricated to verify its ability to regulate phase and absorption. According to the simulation analysis, the number of I-shaped resonators is selected as six, as shown in Figure 16a. The resistivities of the thin-film resistors in the resonators are  $50 \Omega \text{ sq}^{-1}$ . The designed and optimized dimensions of the metamaterial are as follows:  $w_I = 150 \mu\text{m}$ ,  $l_{I1} = l_{I2} = l_{I3} = l_{I5} = 335 \mu\text{m}$ ,  $l_{I4} = 345 \mu\text{m}$ ,  $l_{I6} = 330 \mu\text{m}$ ,  $s_I = 600 \mu\text{m}$ ,  $w_R = g_I = 110 \mu\text{m}$ ,  $l_{\text{sub}} = 8000 \mu\text{m}$ , and  $w_{\text{sub}} = 1052 \mu\text{m}$ . In order to enable fabrication with other quartz substrates with different lengths on the same wafer, the quartz substrate of this design contains a section of blank dielectric for length adjustment. The influence of this blank dielectric on the performance of the metamaterial waveguide is negligible.



**Figure 16.** (a) Dimension identification of the designed quartz substrate. (b) Photographs of the fabricated metamaterial waveguide module.

The photograph of the fabricated metamaterial waveguide module is depicted in Figure 16b. The split blocks of the WR-4.3 waveguide are machined from aluminum alloy with computer numerical control (CNC) technology. The  $50 \mu\text{m}$  thick quartz substrate is directly bonded to the waveguide’s inner wall through silver epoxy. The length of the waveguide is 32 mm, while that of the quartz substrate is 8 mm. Two rows of threaded holes were added outside the narrow walls of the waveguide, which can be considered as electric walls to reduce electromagnetic energy leakage [37].

Figure 17 displays the schematic diagram and the photograph of the measurement system for evaluating the fabricated module’s performance. A vector network analyzer (ZVA67, Rohde & Schwarz, Munich, Germany) with two WR-4.3 (0.17–0.26 THz) frequency extenders was used to measure the phase and S parameters of the fabricated module. The measured and simulated curves are shown in Figure 18. The maximum absorption amplitude of the fabricated metamaterial waveguide is 19.6 dB, occurring at 0.2055 THz. Compared with the simulation result, the measured  $S_{21}$  curve of the I-shaped metamaterial waveguide exhibits an approximately 3 dB decrease and a leftward shift of 2.3 GHz in the absorption frequency. The phase curve is consistent with the simulation results, but the frequency at which the phase shifts occur exhibits similar offsets as the absorption frequency. Additionally, the measured return loss of the metamaterial waveguide is better than 13 dB. Despite the discrepancy between the measured and simulated curves, the results confirm the feasibility of the proposed terahertz metamaterial waveguide in achieving the modulation of the absorption and the phase.

The differences between the measured and simulated results in Figure 18 are mainly caused by insufficient fabrication precision, thin-film resistance errors, and insertion losses of the H-plane splitting waveguides and quartz substrates. Due to the limitations of fabrication processes, thin-film resistance can possess a maximum error of  $\pm 10\%$ , leading to deviations in the phase, amplitude, and absorption frequency. Moreover, the waveguide is split on its H-plane to facilitate the placement of the quartz substrate, which disrupts the surface currents of the waveguide and increases insertion loss. Furthermore, the inaccurate dielectric constant and loss tangent of the quartz substrate around 0.2 THz also cause shifts in the absorption and phase. In future research, these issues could be addressed by enhancing the processing precision of thin-film resistors, introducing more precise model parameters, and conducting iterative design improvements.

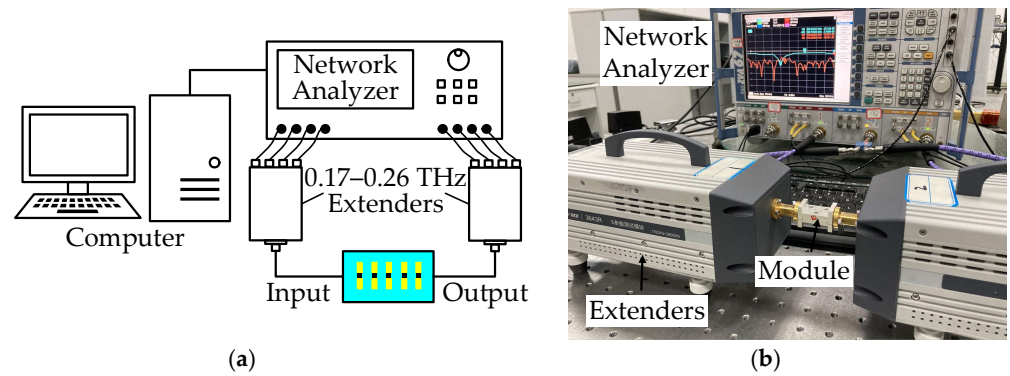


Figure 17. Measurement system. (a) Schematic diagram. (b) Photograph.

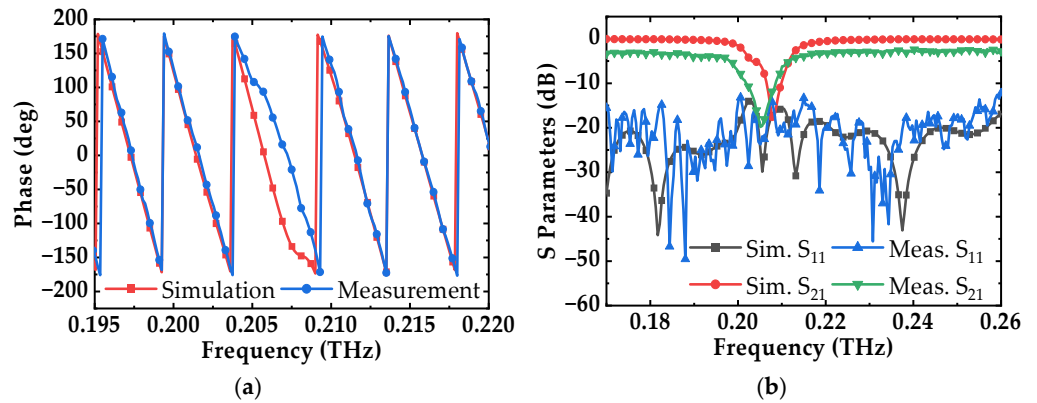


Figure 18. Measured and simulated results. (a) Phase and (b) S parameters of the metamaterial waveguide with I-shaped resonators.

Table 2 compares the proposed metamaterial waveguide in this work and other reported metamaterial waveguides. Most of the reported metamaterial waveguides primarily focus on energy absorption, equalization, and modulation, without considering their control over the phase. The metamaterial waveguide proposed in [41] achieves simultaneous control over absorption and phase. However, its usage of an alumina ceramic substrate with a relatively high dielectric constant and loss tangent makes it challenging to extend its application to higher frequencies.

Table 2. Comparison to other reported metamaterial waveguides.

Reference	Device Type/Function	Frequency (THz)	Substrate	Loss Material	Resonator
[28]	Absorber	0.1	Alumina ceramic	N.A. *	Circular patch
[29]	Energy equalizer	0.1	Alumina ceramic	Film resistor	Square ring
[30]	Amplitude modulator	Terahertz/infrared	Graphene	N.A.	N.A.
[41]	Phase and absorption modulation	0.1	Alumina ceramic	Film resistor	Square ring
This work	Phase and absorption modulation	0.2	Quartz	Film resistor	I-shaped line

\* N.A. represents not applicable.

Compared with other reported metamaterial waveguides, this work utilizes a low-loss and low-dielectric constant quartz substrate, combined with simple I-shaped resonators, to achieve phase and absorption control in the 0.2 THz band. Moreover, this study introduces a method for designing one-dimensional metamaterial waveguides in enclosed spaces based on the analysis results of two-dimensional metamaterials in free space. The metamaterial

waveguide's equivalent medium and circuit models are analyzed. Additionally, this work examines the dimensions of I-shaped resonators and the implementation of resonators of other shapes, analyzing their impact on phase and absorption. The fabrication and measurement of the metamaterial waveguide also provide a positive pre-verification for its potential application in future 0.2 THz communication systems.

## 5. Conclusions

In summary, this paper proposes a metamaterial waveguide with I-shaped resonators to address terahertz systems' phase and amplitude distortions. A simple and effective approach is presented to design one-dimensional metamaterial in an enclosed space based on the analysis results of a two-dimensional metamaterial in free space. By modifying the size and number of the I-shaped resonators, the phase, absorption, and absorption frequency can be effectively adjusted. An analysis of the metamaterial waveguide's phase and absorption control mechanisms is conducted by establishing the equivalent medium model and equivalent circuits. The metamaterial waveguide is designed, fabricated, and measured, and the results show that it has effective phase and amplitude modulation capabilities near 0.2 THz. Additionally, the flexible modulation, simple structure, and easy manufacturing of the proposed metamaterial waveguide make it highly promising for applications in future high-performance terahertz communication systems.

**Author Contributions:** Conceptualization, B.Y. (Bo Yu) and Z.W.; Investigation, B.Y. (Bo Yu), T.Z. and B.Y. (Bo Yan); Methodology, B.Y. (Bo Yu) and Z.W.; Project administration, B.Y. (Bo Yan) and R.X.; Resources, J.Y., Y.S. and T.Z.; Software, B.Y. (Bo Yu), J.Y. and Y.S.; Supervision, T.Z., B.Y. (Bo Yan) and R.X.; Validation, B.Y. (Bo Yu), J.Y. and Y.S.; Visualization, B.Y. (Bo Yan), Z.W. and B.Y. (Bo Yan); Writing—original draft, B.Y. (Bo Yu); Writing—review and editing, B.Y. (Bo Yu), Z.W. and B.Y. (Bo Yan). All authors have read and agreed to the published version of the manuscript.

**Funding:** This research received no external funding.

**Institutional Review Board Statement:** Not applicable.

**Informed Consent Statement:** Not applicable.

**Data Availability Statement:** The authors confirm that the data supporting the findings of this work are available within the article.

**Acknowledgments:** The authors extend sincere gratitude to the 55th Research Institute of China Electronics Technology Corporation (CETC) for their support.

**Conflicts of Interest:** The authors declare no conflict of interest.

## References

1. Wang, C.; Lu, B.; Lin, C.; Chen, Q.; Miao, L.; Deng, X.; Zhang, J. 0.34-THz Wireless Link Based on High-Order Modulation for Future Wireless Local Area Network Applications. *IEEE Trans. Terahertz Sci. Technol.* **2014**, *4*, 75–85. [[CrossRef](#)]
2. Tajima, T.; Song, H.J.; Yaita, M. Compact THz LTCC Receiver Module for 300 GHz Wireless Communications. *IEEE Microw. Wirel. Compon. Lett.* **2016**, *26*, 291–293. [[CrossRef](#)]
3. Cheng, B.B.; Cui, Z.M.; Lu, B.; Qin, Y.L.; Liu, Q.; Chen, P.; He, Y.; Jiang, J.; He, X.Y.; Deng, X.J.; et al. 340-GHz 3-D Imaging Radar With 4Tx-16Rx MIMO Array. *IEEE Trans. Terahertz Sci. Technol.* **2018**, *8*, 509–519. [[CrossRef](#)]
4. Ikari, T.; Sasaki, Y.; Otani, C. 275–305 GHz FM-CW Radar 3D Imaging for Walk-Through Security Body Scanner. *Photonics* **2023**, *10*, 343. [[CrossRef](#)]
5. Kim, Y.; Zhang, Y.; Reck, T.J.; Nemchick, D.J.; Chattopadhyay, G.; Drouin, B.; Chang, M.C.F.; Tang, A. A 183-GHz InP/CMOS-Hybrid Heterodyne-Spectrometer for Spaceborne Atmospheric Remote Sensing. *IEEE Trans. Terahertz Sci. Technol.* **2019**, *9*, 313–334. [[CrossRef](#)]
6. Ding, J.Q.; Shi, S.C.; Zhou, K.; Zhao, Y.; Liu, D.; Wu, W. WR-3 Band Quasi-Elliptical Waveguide Filters Using Higher Order Mode Resonances. *IEEE Trans. Terahertz Sci. Technol.* **2017**, *7*, 302–309. [[CrossRef](#)]
7. Guo, C.; Shang, X.; Lancaster, M.J.; Xu, J.; Powell, J.; Wang, H.; Parow-Souchon, K.; Henry, M.; Viegas, C.; Alderman, B.; et al. A 290–310 GHz Single Sideband Mixer with Integrated Waveguide Filters. *IEEE Trans. Terahertz Sci. Technol.* **2018**, *8*, 446–454. [[CrossRef](#)]
8. Li, Y.L.; Gao, W.; Guo, L.; Chen, Z.H.; Li, C.J.; Zhang, H.M.; Jiao, J.J.; An, B.W. Tunable ultra-broadband terahertz perfect absorber based on vanadium oxide metamaterial. *Opt. Express* **2021**, *29*, 41222–41233. [[CrossRef](#)]

9. Wong, H.; Wang, K.X.; Huitema, L.; Crunteanu, A. Active meta polarizer for terahertz frequencies. *Sci. Rep.* **2020**, *10*, 15382. [[CrossRef](#)]
10. Baig, A.; Gamzina, D.; Kimura, T.; Atkinson, J.; Domier, C.; Popovic, B.; Himes, L.; Barchfeld, R.; Field, M.; Luhmann, N.C. Performance of a Nano-CNC Machined 220-GHz Traveling Wave Tube Amplifier. *IEEE Trans. Electron. Dev.* **2017**, *64*, 2390–2397. [[CrossRef](#)]
11. Jiang, Y.; Lei, W.Q.; Hu, P.; Song, R.; Ma, G.W.; Chen, H.B.; Jin, X. Demonstration of a 220-GHz Continuous Wave Traveling Wave Tube. *IEEE Trans. Electron. Dev.* **2021**, *68*, 3051–3055. [[CrossRef](#)]
12. He, J.W.; He, X.J.; Dong, T.; Wang, S.; Fu, M.X.; Zhang, Y. Recent progress and applications of terahertz metamaterials. *J. Phys. D Appl. Phys.* **2022**, *55*, 123002. [[CrossRef](#)]
13. Yen, T.J.; Padilla, W.J.; Fang, N.; Vier, D.C.; Smith, D.R.; Pendry, J.B.; Basov, D.N.; Zhang, X. Terahertz magnetic response from artificial materials. *Science* **2004**, *303*, 1494–1496. [[CrossRef](#)] [[PubMed](#)]
14. Valentine, J.; Zhang, S.; Zentgraf, T.; Ulin-Avila, E.; Genov, D.A.; Bartal, G.; Zhang, X. Three-dimensional optical metamaterial with a negative refractive index. *Nature* **2008**, *455*, 376–379. [[CrossRef](#)]
15. Schurig, D.; Mock, J.J.; Justice, B.J.; Cummer, S.A.; Pendry, J.B.; Starr, A.F.; Smith, D.R. Metamaterial electromagnetic cloak at microwave frequencies. *Science* **2006**, *314*, 977–980. [[CrossRef](#)]
16. Zhang, X.; Liu, Z.W. Superlenses to overcome the diffraction limit. *Nat. Mater.* **2008**, *7*, 435–441. [[CrossRef](#)]
17. Landy, N.I.; Sajuyigbe, S.; Mock, J.J.; Smith, D.R.; Padilla, W.J. Perfect metamaterial absorber. *Phys. Rev. Lett.* **2008**, *100*, 207402. [[CrossRef](#)]
18. Long, L.V.; Khiem, N.S.; Tung, B.S.; Tung, N.T.; Giang, T.T.; Son, P.T.; Khuyen, B.X.; Lam, V.D.; Chen, L.Y.; Zheng, H.; et al. Flexible Broadband Metamaterial Perfect Absorber Based on Graphene-Conductive Inks. *Photonics* **2021**, *8*, 440. [[CrossRef](#)]
19. Naveed, M.A.; Bilal, R.M.H.; Baqir, M.A.; Bashir, M.M.; Ali, M.M.; Rahim, A.A. Ultrawideband fractal metamaterial absorber made of nickel operating in the UV to IR spectrum. *Opt. Express* **2021**, *29*, 42911–42923. [[CrossRef](#)]
20. Bilal, R.M.H.; Naveed, M.A.; Baqir, M.A.; Ali, M.M.; Rahim, A.A. Design of a wideband terahertz metamaterial absorber based on Pythagorean-tree fractal geometry. *Opt. Mater. Express* **2020**, *10*, 3007–3020. [[CrossRef](#)]
21. Bilal, R.M.H.; Saeed, M.A.; Choudhury, P.K.; Baqir, M.A.; Kamal, W.; Ali, M.M.; Rahim, A.A. Elliptical metallic rings-shaped fractal metamaterial absorber in the visible regime. *Sci. Rep.* **2020**, *10*, 14035. [[CrossRef](#)] [[PubMed](#)]
22. Chen, H.-T.; Padilla, W.J.; Cich, M.J.; Azad, A.K.; Averitt, R.D.; Taylor, A.J. A metamaterial solid-state terahertz phase modulator. *Nat. Photonics* **2009**, *3*, 148–151. [[CrossRef](#)]
23. Rockstuhl, C.; Zhang, W.L. Terahertz phase modulator. *Nat. Photonics* **2009**, *3*, 130–131. [[CrossRef](#)]
24. Zhang, Y.; Qiao, S.; Liang, S.; Wu, Z.; Yang, Z.; Feng, Z.; Sun, H.; Zhou, Y.; Sun, L.; Chen, Z.; et al. Gbps terahertz external modulator based on a composite metamaterial with a double-channel heterostructure. *Nano Lett.* **2015**, *15*, 3501–3506. [[CrossRef](#)] [[PubMed](#)]
25. Pozar, D.M. *Microwave Engineering*, 4th ed.; Wiley: Hoboken, NJ, USA, 2012; 732p.
26. Li, Z.Y.; Kim, M.H.; Wang, C.; Han, Z.H.; Shrestha, S.; Overvig, A.C.; Lu, M.; Stein, A.; Agarwal, A.M.; Loncar, M.; et al. Controlling propagation and coupling of waveguide modes using phase-gradient metasurfaces. *Nat. Nanotechnol.* **2017**, *12*, 675–683. [[CrossRef](#)] [[PubMed](#)]
27. Guo, X.X.; Ding, Y.M.; Chen, X.; Duan, Y.; Ni, X.J. Molding free-space light with guided wave-driven metasurfaces. *Sci. Adv.* **2020**, *6*, eabb4142. [[CrossRef](#)]
28. Wang, Z.G.; Zhou, Y.Q.; Yang, L.M.; Gong, C. Waveguide-based terahertz metamaterial functional components. *J. Phys. D Appl. Phys.* **2017**, *50*, 375107. [[CrossRef](#)]
29. Wang, Z.; Jin, H.; Sun, X.; Li, X.; Xu, Y.; Liu, G.; Gong, C. Meta-waveguide for customizable energy equalization. *Opt. Commun.* **2020**, *474*, 126172. [[CrossRef](#)]
30. Khromova, I.; Andryieuski, A.; Lavrinenko, A. Ultrasensitive terahertz/infrared waveguide modulators based on multilayer graphene metamaterials. *Laser Photonics Rev.* **2014**, *8*, 916–923. [[CrossRef](#)]
31. Bhardwaj, A.; Pratap, D.; Vaibhav Srivastava, K.; Ramakrishna, S.A. Highly Sensitive Permittivity Sensor Using an Inhomogeneous Metamaterial Cylindrical Waveguide. *IEEE Sens. J.* **2021**, *21*, 9120–9127. [[CrossRef](#)]
32. Xue, Y.L.; Liu, W.; Gu, Y.; Zhang, Y. Light storage in a cylindrical waveguide with metamaterials. *Opt. Laser Technol.* **2015**, *68*, 28–35. [[CrossRef](#)]
33. Wells, J. Faster Than Fiber: The Future of Multi-Gb/s Wireless. *IEEE Microw. Mag.* **2009**, *10*, 104–112. [[CrossRef](#)]
34. Hadidian, B.; Khoeini, F.; Naghavi, S.M.H.; Cathelin, A.; Afshari, E. A 220-GHz Energy-Efficient High-Data-Rate Wireless ASK Transmitter Array. *IEEE J. Solid-State Circuits* **2022**, *57*, 1623–1634. [[CrossRef](#)]
35. Rodriguez-Vazquez, P.; Grzyb, J.; Heinemann, B.; Pfeiffer, U.R. A 16-QAM 100-Gb/s 1-M Wireless Link with an EVM of 17% at 230 GHz in an SiGe Technology. *IEEE Microw. Wirel. Compon. Lett.* **2019**, *29*, 297–299. [[CrossRef](#)]
36. Yang, T.; Li, X.Y.; Yu, B.; Gong, C. Design and Print Terahertz Metamaterials Based on Electrohydrodynamic Jet. *Micromachines* **2023**, *14*, 659. [[CrossRef](#)]
37. Jin, J.-M. *Theory and Computation of Electromagnetic Fields*, 2nd ed.; John Wiley & Sons, Inc.: Hoboken, NJ, USA, 2015; 715p.
38. Cheng, D.K. *Field and Wave Electromagnetics*; Addison-Wesley: Reading, MA, USA, 1989; 703p.
39. Ding, K.; Shen, Y.; Ng, J.; Zhou, L. Equivalent-medium theory for metamaterials made by planar electronic materials. *EPL Europhys. Lett.* **2013**, *102*, 28005. [[CrossRef](#)]

40. Huang, X.; Yang, H.; Wang, D.; Yu, S.; Lou, Y.; Guo, L. Calculations of a wideband metamaterial absorber using equivalent medium theory. *J. Phys. D Appl. Phys.* **2016**, *49*, 325101. [[CrossRef](#)]
41. Yan, B.; Yu, B.; Xu, J.F.; Li, Y.K.; Wang, Z.G.; Wang, Z.X.; Yu, B.; Ma, H.Y.; Gong, C. Customized meta-waveguide for phase and absorption. *J. Phys. D Appl. Phys.* **2021**, *54*, 465102. [[CrossRef](#)]
42. Pang, Y.; Cheng, H.; Zhou, Y.; Wang, J. Analysis and design of wire-based metamaterial absorbers using equivalent circuit approach. *J. Appl. Phys.* **2013**, *113*, 114902. [[CrossRef](#)]
43. Pang, Y.-Q.; Zhou, Y.-J.; Wang, J. Equivalent circuit method analysis of the influence of frequency selective surface resistance on the frequency response of metamaterial absorbers. *J. Appl. Phys.* **2011**, *110*, 023704. [[CrossRef](#)]
44. Hu, C.G.; Li, X.; Feng, Q.; Chen, X.N.; Luo, X.G. Investigation on the role of the dielectric loss in metamaterial absorber. *Opt. Express* **2010**, *18*, 6598–6603. [[CrossRef](#)] [[PubMed](#)]
45. Qin, M.; Zhang, L.M.; Wu, H.J. Dielectric Loss Mechanism in Electromagnetic Wave Absorbing Materials. *Adv. Sci.* **2022**, *9*, 2105553. [[CrossRef](#)] [[PubMed](#)]
46. Zhou, J.; Economou, E.N.; Koschny, T.; Soukoulis, C.M. Unifying approach to left-handed material design. *Opt. Lett.* **2006**, *31*, 3620–3622. [[CrossRef](#)] [[PubMed](#)]

**Disclaimer/Publisher’s Note:** The statements, opinions and data contained in all publications are solely those of the individual author(s) and contributor(s) and not of MDPI and/or the editor(s). MDPI and/or the editor(s) disclaim responsibility for any injury to people or property resulting from any ideas, methods, instructions or products referred to in the content.